International Journal of Mechanical, Industrial and Aerospace Sciences
ISSN: 2517-9950
Vol:2, No:1, 2008

Application of H_2-based Sliding Mode Control for an Active Magnetic Bearing System

Abdul Rashid Husain, Mohamad Noh Ahmad, and Abdul Halim Mohd. Yatim

***Abstract*—**In this paper, application of Sliding Mode Control (SMC) technique for an Active Magnetic Bearing (AMB) system with varying rotor speed is considered. The gyroscopic effect and mass imbalance inherited in the system is proportional to rotor speed in which this nonlinearity effect causes high system instability as the rotor speed increases. Transformation of the AMB dynamic model into regular system shows that these gyroscopic effect and imbalance lie in the mismatched part of the system. A H_2-based sliding surface is designed which bound the mismatched parts. The solution of the surface parameter is obtained using Linear Matrix Inequality (LMI). The performance of the controller applied to the AMB model is demonstrated through simulation works under various system conditions.

***Keywords*—**Active Magnetic Bearing (AMB), Sliding Mode Control (SMC), Linear Matrix Inequality (LMI), mismatched uncertainty and imbalance.

I. Introduction

SLIDING Mode Control (SMC) has received great attention in recent years because of its robustness against uncertainties present in system [1], [2] ,[3] and [4]. SMC is a nonlinear control technique that is applicable to a wide range of dynamic system including the linear, nonlinear, multi-input/multi-output, discrete-time and large scale systems. There are many approaches have been reported and considered in the design process of the sliding-mode control law, such that the system is robust or even insensitive to parametric uncertainties and disturbance. In the practical application of SMC, the controller has also been successfully adapted in many forms and applied in numerous real-world applications such as robot manipulator [5], active suspension system [6], magnetic suspension system and magnetic bearings [7][8].

AMB system however is an advance mechatronic system in which it is open loop unstable and inherent high nonlinearity effect. Thus the system requires feedback gain such that the closed-loop system is stable and able to meet required system performance. Although the system is complex in term of its structural and control design, the advantages it offers outweigh the design complexity. Thus stabilization of the system to meet various application needs has offered great challenges to control research group.

The main objective of this work is the application of the SMC technique to the AMB system. The design of SMC controller involves two crucial steps which are commonly referred to as the reaching phase and the sliding phase [1][2]. In this paper, the latter one which is the design of the sliding surface using H_2 guaranteed cost surface based on work in [9] is of more emphasis. The work in [9] is the extension of the surface design reported in [4] and elaborated extensively in [2]. In [10], the application of the H_2 designed surface based on [4] with a new SMC controller into AMB system is explored in which the result shows that the present of mismatched system uncertainties and disturbance may cause degradation of system performance. Thus, based on the surface design outlined in [9] and control law in [2], the performance of the AMB system with the present of the mismatched system uncertainty and disturbance is investigated through simulation work. The design steps as well as the necessary theoretical background are outlined in which based on the final result, it is shown that the proposed method gives an improved system performance.

The outline of this paper is as follows: In Section II, the model of the AMB system based on [8] is illustrated. Section III covers the detail design of sliding surface wherein the optimal parameter is obtained by solving an LMI optimization problem. Then, in Section IV, the performances on the AMB system under the designed controller are illustrated through simulation works under various system conditions. Finally, the conclusion in Section V summarizes the contribution of the work.

II. Modeling of an Active Magnetic Bearing System

In order to synthesize the proposed sliding surface with the controller, a vertical shaft AMB system model for the application of turbo molecular pump system is re-derived based on the work done in [8].

A. Mathematical Model

The gyroscopic effect that causes the coupling between two axes of motions (pitch and yaw). Fig. 1 illustrates the five DOF vertical magnetic bearing in which the vertical axis (z-axis) is assumed to be decoupled from the system and hence

A. R. Husain is with Universiti Teknologi Malaysia (UTM), 81310, Skudai, Johore Malaysia (phone: +607-5535894; fax: +607-5566272; e-mail: rashid@ fke.utm.my).

M. N. Ahmad is with Universiti Teknologi Malaysia (UTM), 81310, Skudai, Johore Malaysia. He is the Head of Dept. Mechatronics and Robotics, Faculty of Elec. Eng., UTM (e-mail: noh@fke.utm.my).

A. H. M. Yatim is with the Universiti Teknologi Malaysia (UTM), 81310, Skudai, Johore Malaysia.. He is the Deputy Dean (Academics), Faculty of Elec. Eng., UTM (e-mail: halim@ieee.org).

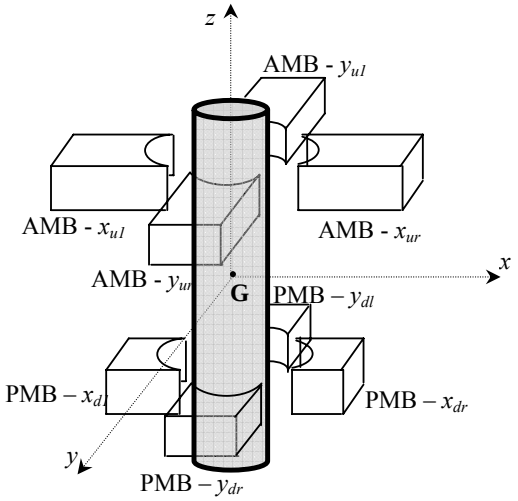

Fig. 1 Vertical Active Magnetic Bearing System

controlled separately. The top part of the rotor of the system in Fig. 1 is controlled actively by the magnetic bearing, labeled as AMB, in which the coil currents are the inputs. The bottom part of the rotor however is levitated to the center of the system by using two sets of permanent magnets labeled as PMB. The rotation of rotor around the *z*-axis is supplied by external driving mechanism and considered as a time-varying parameter.

Fig. 2 illustrates the free-body diagram of the rotor which shows the total forces produced by the AMB and PMB of the system. Based on the principle of flight dynamics [11], the equations of motion of the rotor-magnetic bearing system is as follows:

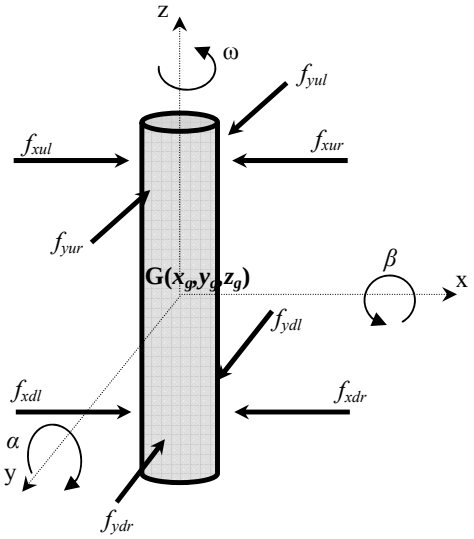

Fig. 2 AMB free-body diagram

$$\begin{aligned} m\ddot{x}_g &= f_{x_u} + f_{x_b} + m_{un} l\omega^2 \cos(\omega t) \\ J_r\ddot{\beta} &= -J_a\omega_z\dot{\alpha} + L_u f_{x_u} - L_b f_{x_b} \\ m\ddot{y}_g &= f_{y_u} + f_{y_b} + m_{un} l\omega^2 \sin(\omega t) \\ J_r\ddot{\alpha} &= J_a\omega_z\dot{\beta} - L_u f_{y_u} + L_b f_{y_b} \end{aligned} \quad (1)$$

The terms $m_{un} l\omega^2 \cos(\omega t)$ and $m_{un} l\omega^2 \sin(\omega t)$ are the imbalances due the difference between rotor geometric center and mass center. These imbalances cause the whirling motion and the magnitude is proportional to the rotor rotational speed, ω. The gyroscopic effect is represented by the term $-J_a\omega_z\dot{\alpha}$ and $J_a\omega_z\dot{\beta}$, where it can be noticed that this will cause the coupling between the axes of motions proportional to the speed. The control forces produced by the AMB are given by the following equations:

$$\begin{aligned} f_{xu} &= 2K_{du}x_g + 2L_u K_{du}\beta + 2K_{iu}I_x \\ f_{yu} &= 2K_{du}y_g - 2L_u K_{du}\alpha + 2K_{iu}I_y \end{aligned} \quad (2)$$

where $f_{xu} = f_{xur} - f_{xul}$ and $f_{yu} = f_{yur} - f_{yul}$ are the net forces produced by the AMB on each *x*- and *y*-axis respectively (the same net force for bottom PMB as well). This is possible by having the AMB coil wound to produce differential current mode. For the PMB, the net forces produced are given by the following equations:

$$\begin{aligned} f_{xb} &= -2C_b\dot{x}_g + 2C_b L_b\dot{\beta} - 2K_b x_g + 2K_b L_b\beta \\ f_{yb} &= -2C_b\dot{y}_g - 2C_b L_b\dot{\alpha} - 2K_b y_g - 2K_b L_b\alpha \end{aligned} \quad (3)$$

Equations (1), (2) and (3) can be integrated to produce the AMB model in the following form:

$$\dot{X}(t) = A(\omega)X(t) + BU(t) + F(\omega,t) \quad (4)$$

where $X = [x_g, \beta, y_g, \alpha, \dot{x}_g, \dot{\beta}, \dot{y}_g, \dot{\alpha}]^T$ are the states of the system, $A(\omega) \in \Re^{8x8}$ is the system matrix, $B \in \Re^{8x2}$ is the input matrix, $U(t) = [I_x \;\; I_y]^T$ the input currents. The nonzero elements of the matrices are shown in the Appendix A. The range of the rotor speed is given below:

$$0 \; rpm \le \omega \le 10{,}000 \; rpm \; . \quad (5)$$

From the dynamic model (4), the uncertainties present in the system are in the system and disturbance matrix which are due to gyroscopic effect and mass imbalance. The parameters of the AMB system are given in Appendix C.

III. H_2-BASED SLIDING MODE CONTROL DESIGN

Consider a class of uncertain system

$$\dot{x}(t) = (A + \Delta A(\omega))x(t) + Bu(t) + Ew(\omega,t) \quad (6)$$

where $x(t) \in \Re^n$ is the system states, $u(t) \in \Re^m$ is the control input and ω is any time-varying scalar function. A and B is the system and input matrices, respectively, and B is of full rank. $\Delta A(\omega)$ represents the uncertainty in the system matrix and matrix E is the disturbance matrix that map the disturbance $w(\omega,t)$ into the system. To complete the description of the uncertain dynamical system, the following assumptions are introduced and assumed to be valid.

A1) The system uncertainty $\Delta A(\omega)$ and the disturbance E are mismatched such that:

$$R(B) \not\subset R(E) + R(\Delta A)$$

A2) The linear model mismatch is supposed to belong to a convex polytope in parameter space such that:

$$\Delta A = \sum_{i=1}^{k} \alpha_i \Delta A_i \ , \ \sum_{i=1}^{k} \alpha_i = 1 \ , \ \alpha_i \geq 0 \ \forall i \in 1,\cdots,k.$$

A3) The pair (A,B) is controllable.
A4) All states are available.

The sliding surface is defined as:

$$\sigma = Cx(t) = 0 \tag{7}$$

where C is the design matrix that determines the desired performance of the $(n\text{-}m)$ reduced-order closed-loop system.

Define an output variable as

$$z(t) = Lx(t) \tag{8}$$

Due to the mismatched condition, the transfer function from the exogenous input vector $w(t)$ to this output $z(t)$ is given by

$$Z(s) = H(s)W(s) \tag{9}$$

where $Z(s)$ and $W(s)$ are the Laplace transform of $z(t)$ and $w(t)$ respectively and $H(s)$ is valid for $t > \tau$. When the system in the sliding motion, the H_2 norm of the transfer function (9) for the closed-loop system is defined as follows:

$$\left\| H(s) \right\|_2^2 = \frac{1}{2\pi} \int_{-\infty}^{\infty} tr[H(j\omega_s) * H(j\omega_s)] d\omega_s \tag{10}$$

From this, as highlighted in [9], the main objective is to find the optimal sliding surface C_{opt}, such that the upper bound of the H_2 norm (10) over all mismatched ΔA such that:

$$C_{opt} = \arg \min_{C} \max_{\Delta A} \Omega(C, \Delta A), \quad \Omega(C, \Delta A) \geq \left\| H(s) \right\|_2 \tag{11}$$

The minimization of the upper bound of $\Omega(C, \Delta A)$ which can be found as the solution of the sliding surface as explained in the following section.

A. Canonical Transformation

The design of the sliding surface is carried by transforming the system dynamic into a regular form and this is in-line with the step outlined in [2][4]. The transformation matrix T is chosen such that

$$TB = \begin{bmatrix} 0 \\ \overline{B}_2 \end{bmatrix}, \ TT^T = \boldsymbol{I} \tag{12}$$

where matrix $\overline{B}_2 \in \Re^{m \times m}$ is nonsingular. Then applying this transformation to system (6), a new system representation is obtained as:

$$\begin{aligned} \overline{x} &= Tx \\ \dot{\overline{x}} &= T(A + \Delta A)T^{-1}\overline{x} + TBu + TEw \\ CT^{-1}\overline{x} &= 0 \\ z &= LT^{-1}\overline{x} \end{aligned} \tag{13}$$

Thus, the system states can be partitioned as follows:

$$\overline{x} = \begin{bmatrix} \overline{x}_1 \\ \overline{x}_2 \end{bmatrix}, \ \overline{x}_1 \in \Re^{n-m} \ , \ \overline{x}_2 \in \Re^m \tag{14}$$

Then, the matrices of the system can be partitioned to form the following new matrices:

$$\begin{aligned} \overline{A} &= TAT^{-1} = \begin{bmatrix} \overline{A}_{11} & \overline{A}_{12} \\ \overline{A}_{21} & \overline{A}_{22} \end{bmatrix}, \\ \overline{\Delta A} &= TAT^{-1} = \begin{bmatrix} \overline{\Delta A}_{11} & \overline{\Delta A}_{12} \\ \overline{\Delta A}_{21} & \overline{\Delta A}_{22} \end{bmatrix}, \\ \overline{E} &= TE = \begin{bmatrix} \overline{E}_1 \\ \overline{E}_2 \end{bmatrix}, \\ \overline{C} = CT^{-1} &= \begin{bmatrix} \overline{C}_1 & \overline{C}_2 \end{bmatrix} \text{ and } \overline{L} = LT^{-1} = \begin{bmatrix} \overline{L}_1 & \overline{L}_2 \end{bmatrix} \end{aligned} \tag{15}$$

Following the same procedure in [2], the surface equation becomes

$$\overline{C}_1\overline{x}_1 + \overline{C}_2\overline{x}_2 = 0 \tag{16}$$

By knowing that $\det(\overline{C}_2) \neq 0$, this will lead to

$$\overline{x}_2 = -\overline{C}_2^{-1}\overline{C}_1\overline{x}_1 \tag{17}$$

To simplify the derivation, the following terms are introduced which are:

$$F \triangleq \overline{C}_2^{-1}\overline{C}_1,$$

$$\Phi \underline{\underline{\Delta}} \overline{A}_{11} + \overline{\Delta A}_{11},$$
$$\Gamma \underline{\underline{\Delta}} \overline{A}_{12} + \overline{\Delta A}_{12}. \quad (18)$$

From (15), (16) and these new terms, the new representation of the reduced-order closed-loop system is obtained as follows:

$$\begin{aligned} \dot{\bar{x}}_1 &= \Phi \bar{x}_1 + \Gamma \bar{x}_2 + \overline{E}_1 w \\ \bar{x}_2 &= -F \bar{x}_1 \\ z &= \overline{L}_1 \bar{x}_1 + \overline{L}_2 \bar{x}_2 \end{aligned} \quad (19)$$

Thus, viewing this closed-loop system, it is obvious that the design of the sliding surface is equivalent to designing feedback gain, *F*, for the reduced-order system with uncertainties. Looking at the assumption *A2)*, the matrices $\Phi \underline{\underline{\Delta}} \overline{A}_{11} + \overline{\Delta A}_{11}$ and $\Gamma \underline{\underline{\Delta}} \overline{A}_{12} + \overline{\Delta A}_{12}$ also belongs to a polytope-type set with known vertices. The set can be defined as follows:

$$\wp \underline{\underline{\Delta}} \left\{ \langle \Phi, \Gamma \rangle = \sum_{i=1}^{k} \alpha_i \langle \Phi_i, \Gamma_i \rangle, \sum_{i=1}^{k} \alpha_i = 1, \alpha_i \geq 0 \right\} \quad (20)$$

The vertices of this polytope (20) corresponds to he vertices of the uncertain defined in *A2)* in obtained by using the transformation matrix *T*.

B. H_2 Guaranteed Cost Sliding Surface Design

By following the design step outline in [9], an assumption on the matrix *L* in (8) is introduced in which the assumption will guarantee that the H_2 cost function optimization for the sliding surface design is nonsingular. The assumption is as follows:

$$\overline{L}_2^T \overline{L}_2 > 0 \quad (21)$$

As discussed in the next section, although for AMB system that the freedom of choosing the matrix *L* is quite flexible, the velocities of the gap displacements are also required to fulfill this condition and thus to avoid singularity problem in finding the solution. In practical point of view, getting the velocities of the gap is expensive and may cause some constraints. In this work, however, only the theoretical aspect is concerned and as imposed by assumption *A4)* this requirement has not put any limitation in obtaining the final result.

Then, with this assumption (21), a new variable is introduced as follows:

$$e(t) = (\overline{L}_2^T \overline{L}_2)^{-1} \overline{L}_2^T \overline{L}_2 \bar{x}_1 + \bar{x}_2 \quad (22)$$

The reduced-order system (19) may be written in term of $\bar{x}_1$ and *e* as

$$\dot{\bar{x}}_1 = (\Phi - \Gamma (\overline{L}_2^T \overline{L}_2)^{-1} \overline{L}_2^T \overline{L}_1) \bar{x}_1 + \Gamma e + \overline{E}_1 w$$

$$z = (\overline{L}_1 - \overline{L}_2 (\overline{L}_2^T \overline{L}_2)^{-1} \overline{L}_2^T \overline{L}_1) \bar{x}_1 + \overline{L}_2 e \quad (23)$$

Furthermore, the system can be simplified by defining the following terms:

$$\begin{aligned} \overline{\Phi} &= \Phi - \Gamma (\overline{L}_2^T \overline{L}_2)^{-1} \overline{L}_2^T \overline{L}_1 \\ \Lambda &= \overline{L}_1 - \overline{L}_2 (\overline{L}_2^T \overline{L}_2)^{-1} \overline{L}_2^T \overline{L}_1 \end{aligned} \quad (24)$$

Then, the transformed uncertainty polytope (20) can be recast as:

$$(\overline{\Phi}, \Gamma) \in \aleph \Leftrightarrow (\Phi, \Gamma) \in \wp$$
$$\overline{\Phi}_i = \Phi_i - \Gamma_i \overline{L}_2 (\overline{L}_2^T \overline{L}_2)^{-1} \overline{L}_2^T \overline{L}_1, \quad \forall i = 1, \cdots, k \quad (25)$$

From (19) and (22), the transformed gain matrix is

$$\begin{aligned} e(t) &= (-F + (\overline{L}_2^T \overline{L}_2)^{-1} \overline{L}_2^T \overline{L})_2 \bar{x}_1 \\ &= K \bar{x}_1 \end{aligned} \quad (26)$$

Consider now the set Ξ of the symmetric positive-definite matrices X such that:

$$\Xi : \{ X \in \Re^{(n-m)\times(n-m)} \mid X = X^T > 0;$$
$$(\overline{\Phi} - \Gamma K) X + X (\overline{\Phi} - \Gamma K)^T + \overline{E}_1 \overline{E}_1 \leq 0, \ \forall (\overline{\Phi}, \Gamma) \in \aleph \} \quad (27)$$

For an arbitrary but fixed pair of $(\overline{\Phi}, \Gamma) \in \aleph$, the H_2 norm of system (23) is bounded by:

$$\| H(s) \|_2^2 \leq tr((\Lambda - \overline{L}_2 K) X (\Lambda - \overline{L}_2 K)^T), \quad \forall X \in \Xi. \quad (28)$$

Let a new matrix $W \in \Xi$, then a new variable can be defined as

$$Z = KW, \ \therefore K = ZW^{-1} \quad (29)$$

Thus, the problem of minimization of the upper bound of the H_2 norm (28) can be represented as

$$\min \ tr(\Lambda W \Lambda^T + \overline{L}_2 Z W^{-1} Z^T \overline{L}_2^T)$$

s. t.:

$$\overline{\Phi} W - \Gamma Z + W \overline{\Phi}^T - Z^T \Gamma^T + \overline{E}_1 \overline{E}_1^T \leq 0, \ \forall (\overline{\Phi}, \Gamma) \in \aleph. \quad (30)$$

Obviously, this problem can be expressed as LMI problem [12]. Defining the objective function in (30) as a new variable as follows:

$$Q \geq \Lambda W \Lambda^T + \overline{L}_2 Z W^{-1} Z^T \overline{L}_2^T \quad (31)$$

Taking the Schur complement of (31), then, the problem can be represented as and LMI optimization problem:

$$\Omega^2 = \min_{W,Z,Q} \ tr(Q)$$

$$\text{s. t. :} \begin{cases} \begin{bmatrix} W & Z^T\overline{L}_2^T \\ \overline{L}_2 Z & Q-\Lambda W\Lambda^T \end{bmatrix} \geq 0 \\ W>0 \\ \overline{\Phi}_i W + W\overline{\Phi}_i - \Gamma_i Z - Z^T\Gamma_i^T + \overline{E}_1\overline{E}_1^T \leq 0, \\ \forall i = 1,\cdots,k. \end{cases} \tag{32}$$

If the solution of (32) is feasible, then Theorem 1 in [9] hold and the sliding surface parameter that guarantees the existence of the optimal upper bound H_2 norm can be obtained. With the values of W and Z determined, as stated in the theorem, the gain K in (29) can be obtained and lead to the optimal surface values as follows:

$$C_{opt} = \left[\overline{C}_2((\overline{L}_2^T L_2)^{-1}\overline{L}_2^T\overline{L}_1 - K) \quad \overline{C}_2\right]T \tag{33}$$

Notice that the matrix $\overline{C}_2$ does not have any influence in the reduced order system and can be chosen freely provided it is full rank and $\overline{C}_2 = I$ is a convenient as stated in [2][4][9].

C. Control Law

The next phase in the design phase of sliding mode control is to propose a control law that can ensure the reachability condition is met. For this work, the control law in [2] is adapted as follows:

$$u(t) = -(CB)^{-1}CAx(t) - \rho\, sign(Cx(t)) \tag{34}$$

where ρ is any small positive constant to bound matched uncertainties. The proof of the reachability condition can be found in [2] and purposely not shown here.

IV. Simulation on AMB System and Discussion

The simulation work is performed by using MATLAB® and Simulink®. For solving the LMI problem (32), instead of using standard LMI Toolbox in Matlab, YALMIP/SeDuMi convex problem solver for semi-definite problem is used [13][14]. YALMIP/SeDuMi is among the newly developed convex problem solver which is proven to produce a less conservative solution and a higher convergence rate. The procedure of designing the sliding surface of the controller and its application on the AMB system is outlined as follows:

***Step 1*:** Choose the output matrix L. For this work two output matrix L are chosen as follows:

$$L_s = \begin{bmatrix} 1 & 1 & 0 & 0 & 1 & 0 & 0 & 0 \\ 0 & 0 & 1 & 1 & 0 & 0 & 1 & 0 \end{bmatrix},$$

$$L_b = \begin{bmatrix} 1 & 0 & 0 & 0 & 0 & 0 & 0 & 0 \\ 0 & 1 & 0 & 0 & 0 & 0 & 0 & 0 \\ 0 & 0 & 1 & 0 & 0 & 0 & 0 & 0 \\ 0 & 0 & 0 & 1 & 0 & 0 & 0 & 0 \\ 0 & 0 & 0 & 0 & 1 & 1 & 0 & 0 \\ 0 & 0 & 0 & 0 & 0 & 0 & 1 & 1 \end{bmatrix}.$$

The reason to choose two output matrices is to demonstrate how the performance of the controller is significantly affected by the structure of L. Specifically for this AMB system, the practically desired outputs can be obtained by linear combination of the system states in which this provides great freedom to choose the structure of matrix L. Thus, both of these matrices are valid for this system as long as the assumption that all the states are available is valid.

***Step 2*:** Obtain the orthonormal transformation matrix using QR decomposition which is as follows:

$$T = \begin{bmatrix} 0 & 0 & 1 & 0 & 0 & 0 & 0 & 0 \\ 0 & 0 & 0 & 1 & 0 & 0 & 0 & 0 \\ -0.1844 & 0 & 0 & 0 & 0.9660 & -0.1812 & 0 & 0 \\ -0.9829 & 0 & 0 & 0 & -0.1812 & 0.0340 & 0 & 0 \\ 0 & -0.1844 & 0 & 0 & 0 & 0 & 0.9660 & 0.1812 \\ 0 & 0.9829 & 0 & 0 & 0 & 0 & 0.1812 & 0.0340 \\ 0 & 0 & 0 & 0 & -0.1844 & -0.9829 & 0 & 0 \\ 0 & 0 & 0 & 0 & 0 & 0 & -0.1844 & 0.9829 \end{bmatrix}$$

Note that the transformation matrix is not unique. As outlined previously the chosen T must fulfill the requirement (12).

***Step 3*:** Transform the system into regular form and find the matrices $\Phi_1, \Phi_1, \Gamma_1, \Gamma_2, \overline{\Phi}_1, \overline{\Phi}_2$ and Λ.

After performing the transformation into reduced-order system, the set of matrices using each L_s and L_b are obtained. Due to page limitation, only the matrices obtained from L_s are included in this paper. The matrices that belong to L_b can be obtained in the same manner. The matrices for L_s are shown in Appendix B.

***Step 4*:** Solve LMI set (32) for K and C_{opt} from (33). By using the YALMIP/SeDuMi LMI solver, the calculated parameters are as follows:

$$K = \begin{bmatrix} -2.7145 & 0.0031 & -0.0329 & -0.1753 & 0.0032 & -0.0170 \\ 88.7157 & -0.0405 & 0.1228 & 0.6545 & -0.0251 & 0.1278 \end{bmatrix}$$

$$C = \begin{bmatrix} -5.6019 & -5.4063 & 2.7145 & -0.0031 & -5.4236 & 0 & 0 & 0 \\ 0.6659 & -0.1302 & -94.1392 & -5.3830 & 0 & 0 & -5.4224 & 0.0002 \end{bmatrix}$$

With this C matrix available, by using the control law (34), the complete closed-loop system can be simulated. The initial values of the states are set at $[x_g, \beta, y_g, \alpha, \dot{x}_g, \dot{\beta}, \dot{y}_g, \dot{\alpha}]^T = [8\times10^{-6}$ m, 0, 20×10^{-6} m, 0, 0, 0, 0, $0]^T$. The system is run at two rotor speeds which are 6000 rpm and 10000rpm. As highlighted in [8], the high resonant speed occurs at 6000 rpm in which the radius of the whirling motion of the rotor is the biggest. The value ρ = 0.8 is selected for all simulation work. As a comparison, the result obtained in [8] as shown in Fig. 3 is used for benchmarking in which the rotor orbit is about 95 micron in diameter.

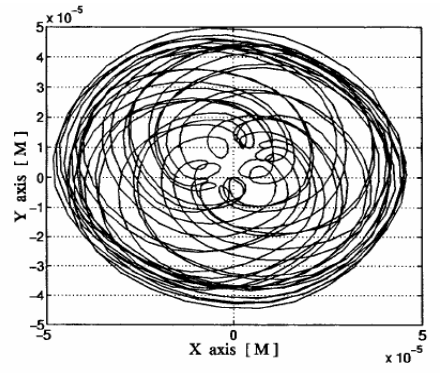

Fig. 3 Rotor orbit at ω = 6000rpm [8]

When the rotor speed is set at ω = 6000rpm, Fig. 4 shows the trajectories of the states X and Y and the rotor orbit when the output matrix L_s is used. It can be seen that the system is approaching asymptotic stability and almost not whirling motion occurs at steady state. When the output matrix is L_b chosen, the rotor orbit of about 12 micron is produced at steady state as shown in Fig. 5. This is a reduction of 87% of rotor orbit compared to Fig. 3. The different between Fig. 4 and Fig. 5 is due the structure of $\bar{L}_2$ imposed by assumption (21). Both L_s and L_b fulfill this requirement, however, from this result the solution of the LMI set with $\bar{L}_2$ designed based on L_s gives a significantly reduced rotor orbit diameter which is approaching zero.

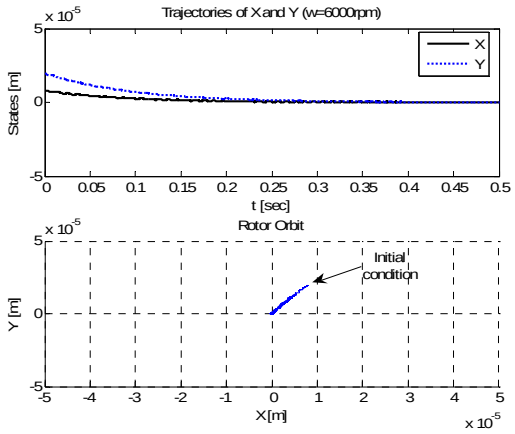

Fig. 4 X and Y trajectories (top) and rotor orbit (bottom) using L_s at ω = 6000rpm

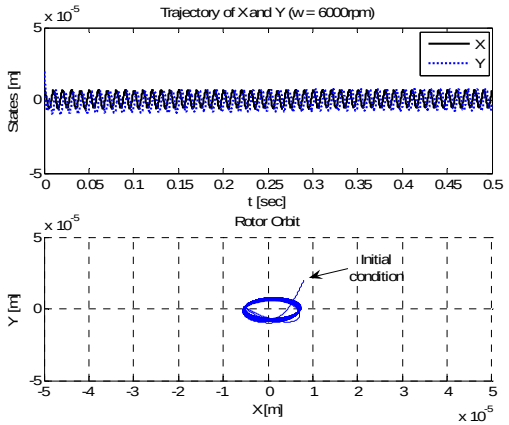

Fig. 5 X and Y trajectories (top) and rotor orbit (bottom) using L_b at ω = 6000rpm

To further assess the performance of the system, Fig. 6 shows the trajectories of X and Y and the rotor orbit with L_s and rotor speed of ω = 10000rpm. It can be noticed that the system response is almost similar to the response when running at ω = 6000rpm in which the system is approach zero diameter of rotor orbit. For the surface parameter with L_s selected, the system response is shown in Fig. 7 where the rotor orbit is about 30 micron. This demonstrates that with the present of the mismatched uncertainties and disturbance, the system response still achieves at the worst the bounded stability as constrained by the designed surface.

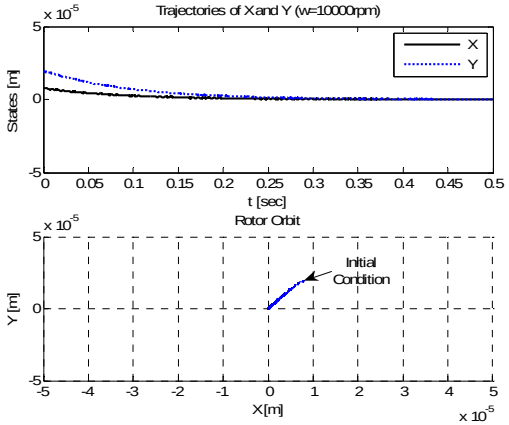

Fig. 6 X and Y trajectories (top) and rotor orbit (bottom) using L_s at ω = 10000rpm

The sliding surfaces σ_1 and σ_2 are shown in Fig. 8 where both surfaces are maintaining at the neighbourhood of ideal sliding surface, $\sigma = 0$. The non-smooth sliding motion is due to the present of the mismatched uncertainties and the imbalance of the AMB system in which this mismatched effect has forced the system to slide off the ideal sliding surface and remain in the designed sliding surface. The control current I_x and I_y is shown in Fig. 9 in which the chattering effect is due to the signum function in the control

law There are many methods reported to eliminate the chattering effect, however, it is insignificant in this work and purposely not covered.

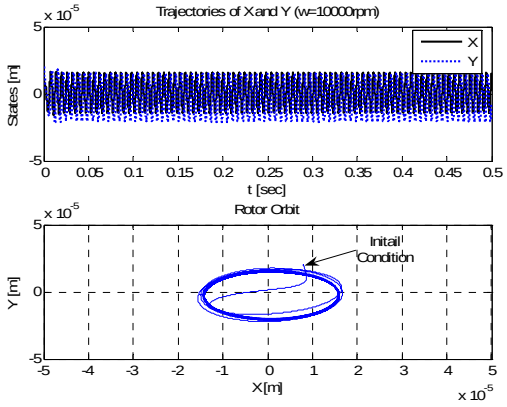

Fig. 7 X and Y trajectories (top) and rotor orbit (bottom) using L_b at ω = 10000rpm

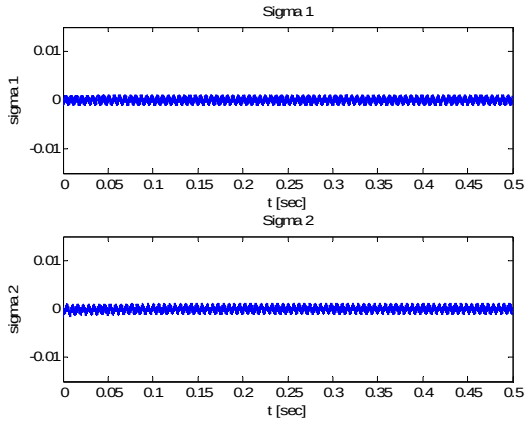

Fig. 8 The sliding surface σ_1 and σ_2 for L_s at ω = 10000rpm

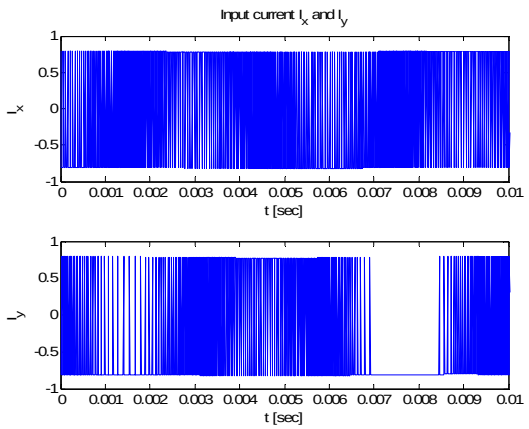

Fig. 9 Current I_x (top) and I_y (bottom)

V. Conclusion

In this work, an application of a SMC controller with H_2 guaranteed cost switching function into AMB system is performed. The proposed controller is proven to be able to achieve the proposed H_2 norm bounded stability at a wide range of rotational rotor speed although with the present of mismatched and matched system uncertainty. The performance of the controller is demonstrated through various simulation works.

Appendix A

The nonzero elements of matrix $A(\omega,t)$, B where i and j indicate the i-th and j-th entry of each element.

$$a_{51}=\frac{2(K_{du}-K_b)}{m}, a_{52}=\frac{2(L_uK_{du}-L_bK_b)}{m}, a_{55}=\frac{2C_b}{m}, a_{56}=\frac{2C_bL_b}{m},$$
$$a_{61}=\frac{2(L_uK_{du}-L_bK_b)}{J_r}, a_{62}=\frac{2(L_u^2K_{du}-L_b^2K_b)}{J_r}, a_{65}=\frac{2L_bC_b}{J_r},$$
$$a_{66}=\frac{2L_b^2C_b}{J_r}, a_{68}=\frac{J_a}{J_r}p, a_{73}=\frac{2(K_{du}-K_b)}{m}, a_{74}=\frac{2(L_uK_{du}+L_bK_b)}{m},$$
$$a_{77}=\frac{2C_b}{m}, a_{78}=\frac{2C_bL_b}{m}, a_{83}=\frac{2(L_uK_{du}+L_bK_b)}{J_r}, a_{84}=\frac{2(L_u^2K_{du}-L_b^2K_b)}{J_r},$$
$$a_{86}=\frac{J_a}{J_r}p,\ a_{87}=\frac{2L_bC_b}{J_r}, a_{68}=\frac{2L_b^2C_b}{J_r}, b_{51}=b_{72}=\frac{2K_{iu}}{m}, b_{61}=-b_{82}=\frac{2L_uK_{iu}}{J_r}.$$
$$f_5=\frac{m_{un}}{m}l\omega^2\cos(\omega t), f_7=\frac{m_{un}}{m}l\omega^2\sin(\omega t)\cdot$$

Appendix B

Elements of matrices $\Phi_1, \Phi_1, \Gamma_1, \Gamma_2, \overline{\Phi}_1, \overline{\Phi}_2$ and Λ for L_s.

$$\Phi_1=10^5\begin{bmatrix}0&0&0&0&0&0\\0&0&0&0&0&0\\0&0&1.6930&9.0314&-0.1427&0.7614\\0&0&-0.3176&-1.6943&0.0268&-0.1428\\-9.1888&-0.7746&-0.0001&0&-0.0043&-0.0008\\-1.7238&-0.1453&0&0&-0.0008&-0.0002\end{bmatrix}$$

$$\Phi_2=10^5\begin{bmatrix}0&0&0&0&0&0\\0&0&0&0&0&0\\0&0&1.6930&9.0314&-0.1425&0.7614\\0&0&-0.3176&-1.6943&0.0267&-0.1428\\-9.1888&-0.7746&-0.0003&0.0001&-0.0043&-0.0008\\-1.7238&-0.1453&-0.0001&0&-0.0008&-0.0002\end{bmatrix}$$

$$\Gamma_1=\begin{bmatrix}&-0.1844\\&0.9829\\-15.0694&78.3917\\3.0146&-14.7061\\-78.2104&44.7795\\-15.6721&8.4005\end{bmatrix}, \Gamma_2=\begin{bmatrix}&-0.1844\\&0.9829\\-15.0694&156.78337\\3.0146&-29.41221\\-156.60214&44.7795\\-30.37821&8.4005\end{bmatrix},$$

$$\overline{\Phi}_1 = 10^5 \begin{bmatrix} 0 & 0 & 0 & 0 & 0 & 0 \\ 0.0001 & 0.0001 & 0 & 0 & 0.0001 & 0 \\ 0.0043 & 0.0043 & 1.6924 & 9.0314 & -0.1384 & 0.7613 \\ -0.0008 & -0.0008 & -0.3175 & -1.6945 & 0.0260 & -0.1428 \\ -9.1863 & -0.7722 & -0.0035 & 0.0050 & -0.0012 & -0.0045 \\ -1.7233 & -0.1449 & -0.0007 & 0.0010 & -0.0002 & -0.0009 \end{bmatrix}$$

$$\overline{\Phi}_2 = 10^5 \begin{bmatrix} 0 & 0 & 0 & 0 & 0 & 0 \\ 0.0001 & 0.0001 & 0 & 0 & 0.0001 & 0 \\ 0.0085 & 0.0085 & 1.6924 & 9.0314 & -0.1342 & 0.7613 \\ -0.0006 & -0.0016 & -0.3175 & -1.6945 & 0.0252 & -0.1430 \\ -9.1863 & -0.7722 & -0.0069 & 0.0099 & -0.0004 & -0.0087 \\ -1.7233 & -0.1449 & -0.0013 & 0.0019 & -0.0001 & -0.0017 \end{bmatrix}$$

$$\Lambda = 10^{-15} \begin{bmatrix} 0 & 0 & 0 & 0 & 0 & 0 \\ -0.2220 & -0.2220 & 0 & 0 & -0.2220 & -0.0278 \end{bmatrix}$$

APPENDIX C

TABLE I
PARAMETER FOR AMB SYSTEM [8]

Symbol	Parameter	Value	Unit
m	Mass of Rotor	1.595	kg
J_a	Moment of Inertia about rotational axis	1.61×10^{-3}	kg.m^2
J_r	Moment of Inertia about radial axis	3.83×10^{-3}	kg.m^2
L_u	Distance of upper AMB to G	0.0128	m
L_b	Distance of lower PMB to G	0.0843	m
K_{iu}	Linearized force/current factor	200	N/A
K_{du}	Linearized force/displ. factor	2.8×10^5	N/m
K_b	Stiffness coefficient of PMB	1.0×10^5	N/m
C_b	Damping coefficient of PMB	48	kg/s
m_{un}	Static imbalance	0.6×10^{-3}	m
l	Distance of unbalance mass from G	0.02	m
ω	Rotor rotational speed	0 – 1047 (0 – 10000)	rad/sec (rpm)

ACKNOWLEDGMENT

The financial support by Ministry of Science, Technology and Innovation, Malaysia (MOSTI) and Universiti Teknologi Malaysia (UTM)) under the E-Science fund under Vot. No. 79014 managed by Research Management Unit (RMC) is acknowledged. A. R. Husain also would like to thank Didier Henrion (LAAS-CNRS, Toulouse) for introducing YALMIL/SeDuMi LMI solver.

REFERENCES

[1] J. Y. Hung, W. B. Gao, and J. C. Hung, "Variable Structure control: A Survey," *IEEE Trans. Industrial. Electronics*, vol. 40, no. 1, pp. 2-22., 1993.

[2] S. Spurgeon, and C. Edwards, *Sliding Mode Control: Theory and Applications*. London: Taylor and Francis, 1998.

[3] X. Li, and R. A. DeCarlo, "Robust Sliding Mode Control of Uncertain Time Delay Systems," *Int. J. Control*, vol. 76, no. 13, pp. 1296-1305, 2003.

[4] V. I. Utkin and K. D. Young, "Methods for constructing discontinuity planes in multidimensional variable structure systems," *Autom. Remote Contr*., vol. 39, pp. 1466-1470, 1978.

[5] M. N. Ahmad, J. H. S. Osman, and M. R. A. Ghani, "Proportional-Integral Sliding Mode Tracking Controller with Application to a Robot Manipulator," in *7th Conf. on Contr., Auto., Rob and Sys., ICARCV*, Singapore, 2003, pp. 863-868.

[6] Y. M. Sam, and J. H. S. Osman, "Modeling and Control of Active Suspension System Using Proportional Integral Sliding Mode Approach," *Asian Jour. Contr*., vol. 7, no. 2, pp. 91-98, 2005.

[7] J. H. Lee, P.E. Allaire, G. Tao, J. A. Decker, and X. Zhang, "Experimental Study of Sliding Mode Control for a Benchmark Magnetic Bearing System and Artificial Heart Pump Suspension," *IEEE Trans. on Contr. Sys. Mag*, vol. 11, no. 1, pp. 128-138, 2003.

[8] S. Sivrioglu, and K. Nonami, "Sliding Mode Control With Time-Varying Hyperplane for AMB Systems," *IEEE/ASME Trans. on Mechatronics*, vol. 3, no. 1, pp. 51-59, 1998.

[9] R. H. C. Takahashi and P. L. D. Peres, "H_2 Guaranteed Cost-switching Surface Design for Sliding Modes with Nonmatching Disturbances", *IEEE Trans. on Auto. Contr*., vol. 44, no. 11, pp. 2214-2218, 1999.

[10] A. R. Husain, M. N. Ahmad and A. H. M. Yatim, "Sliding Mode Control with Linear Quadratic Hyperplane Design: An Application to an Active Magnetic Bearing System", in *5th Student Conf. on Research and Development, SCOReD*, Kuala Lumpur, 2007.

[11] F. Matsumura, and T. Yoshimoto, "System modeling and control design of a horizontal shaft magnetic bearing system," *IEEE Trans. Magnetics*, vol. MAG-22, no. 3, pp. 196-203, May 1986.

[12] S. Boyd, L. El. Ghaoui, E. Feron, and V. Balakrishnan, *Linear Matrix Inequality in Systems and Control Theory*, Philadelphia: SIAM, vol. 15, 1994.

[13] J. Lofberg, "YALMIP: A Toolbox for Modeling and Optimization in {MATLAB}", in *Proc. of the CACSD Conf*., Taiwan, 2004. [Online]. Available: http://control.ee.ethz.ch/~joloef/yalmip.php.

[14] J. F. Sturm, "Using SeDuMi 1.02, a MATLAB toolbox for optimization over symmetric cones," *Optimization Methods and Software- Special issue on Interior Point Methods*, pp. 625-653, 1999. [Online]. Available: http://sedumi.mcmaster.ca.